Buckley, R. M. *et al*. (2024). *Géotechnique* **74**, No. 6, 570–583 [https://doi.org/10.1680/jgeot.22.00044]

Axial cyclic loading of piles in low-to-medium-density chalk

RÓISÍN M. BUCKLEY*, RICHARD J. JARDINE†, STAVROULA KONTOE‡, TINGFA LIU§, BYRON W. BYRNE||, ROSS A. MCADAM¶, FABIAN SCHRANZ** and KEN VINCK††

Comprehensive field investigations into the axial cyclic loading behaviour of open steel pipe piles driven and aged in low-to-medium-density chalk identify the conditions under which behaviour is stable, unstable or metastable. Post-cycling monotonic tests confirmed that stable cycling enhanced pile capacity marginally, while unstable cases suffered potentially large losses of shaft capacity. Metastable conditions led to intermediate outcomes. The patterns by which axial deflections grew under cyclic loading varied systematically with the normalised loading parameters and could be captured by simple fitting expressions. Cyclic stiffnesses also varied with loading conditions, with the highest operational shear stiffnesses falling far below the in situ seismic test values. The monotonic and cyclic axial responses of the test piles were controlled by the behaviour of, and conditions within, the reconsolidated, de-structured, chalk putty annuli formed around pile shafts during driving. Fibre-optic strain gauges identified progressive failure from the pile tip upwards. Large factors of safety were required for piles to survive repetitive loading under high-level, two-way conditions involving low mean loads, while low-amplitude one-way cycling had little impact. A simple 'global' prediction procedure employing interface shear and cyclic triaxial tests is shown to provide broadly representative predictions for field behaviour.

KEYWORDS: chalk; cyclic loading; driven piles; life cycle assessment / life cycle analysis / LCA; marine geotechnics; offshore renewable energy

INTRODUCTION

Chalk outcrops over a wide area of northern Europe and in other regions worldwide. Bridge, port, offshore and other structures constructed at chalk sites often rely on open-ended driven steel pile foundations that may sustain significant load cycling. Offshore structures experience repetitive wind and wave loads, while wind turbines impose tens of millions of blade rotation load cycles.

The impact of cyclic loading on piles driven in chalk appears potentially significant. Burland & French (1990) report a one-way axial cyclic test in Luton, UK, which reduced the tension capacity of a small steel pile by 60% within 20 cycles. Steel 762 mm dia. piles driven at St Nicholas-at-Wade (SNW, near Margate in Kent, UK) which had been tested to failure 19 months earlier (Ciavaglia *et al*., 2017a, 2017b) showed up to 93% shaft capacity losses after modest numbers (N) of two-way axial cyclic loading cycles (Buckley, 2018; unpublished 2013 report by Iberdrola, 'Research project: onshore pile tests in chalk: two-way cyclic axial loading'). However, Lahrs & Kallias (2013) report that cyclic loading applied to a 1·5 m dia. steel tubular pile driven at Hemmoor, Germany led to essentially stable outcomes, although their test pile had undergone dynamic re-strike tests between its installation and cyclic testing. Further research was clearly required; the current paper reports two comprehensive studies into the conditions under which axial cyclic loading affects load-carrying performance negatively and shows how its effects may be assessed in practice.

Recent research into driven pile behaviour in chalk

Considerable difficulties exist in understanding and predicting the monotonic or cyclic behaviour of piles driven in chalk. Jardine *et al*. (2018) identified the poor reliability of industry standard design methods and emphasised the wide ranges of outcomes observed in the field. They summarised findings from limited monotonic and dynamic field-testing programmes they conducted in low-to-medium-density chalks at SNW and the Wikinger Baltic Sea offshore windfarm, noting the following points.

(*a*) Chalk de-structures under percussive driving and forms very soft putty annuli around pile shafts. Very low local shaft resistances develop that fall steeply with increasing relative pile tip depth, h/R.
(*b*) Marked shaft capacity gains, or set-up, develop as piles age after driving.
(*c*) Local tip and shaft radial effective stresses vary directly with cone penetration test (CPT) tip resistance q_t.
(*d*) Local shaft resistances are governed by a Coulomb law, with interface shear angles that can be measured in laboratory interface shear tests.
(*e*) Constrained interface dilation also contributes to shaft resistance.

Manuscript received 3 February 2022; revised manuscript accepted 7 February 2023. First published online ahead of print 20 March 2023.
Discussion on this paper closes on 1 September 2024, for further details see p. ii.
Published with permission by Emerald Publishing Limited under the CC-BY 4.0 license. (http://creativecommons.org/licenses/by/4.0/)
* James Watt School of Engineering, University of Glasgow, Glasgow, UK (Orcid:0000-0001-5152-7759).
† Department of Civil and Environmental Engineering, Imperial College London, London, UK (Orcid:0000-0001-7147-5909).
‡ Department of Civil Engineering, University of Patras, Rio, Greece (Orcid:0000-0002-8354-8762).
§ Department of Civil Engineering, University of Bristol, Bristol, UK (Orcid:0000-0002-5719-8420).
|| Department of Engineering Science, Oxford University, Oxford, UK (Orcid:0000-0002-9704-0767).
¶ Ørsted Wind Power, London, UK (Orcid:0000-0003-0292-3549).
** Office of the Tyrolean Regional Government, Innsbruck, Austria (Orcid:0000-0001-8871-091X).
†† Department of Civil and Environmental Engineering, Imperial College London, London, UK (Orcid:0000-0002-0990-0895).

Downloaded by [] on [30/05/24]. Published with permission by the ICE under the CC-BY license

(*f*) The CPT-based, effective stress, Chalk Imperial College Pile (ICP)-18 axial capacity framework (Jardine *et al*., 2018) appeared to capture the above features adequately, although further field research was required to develop reliable practical design procedures.

Buckley *et al*. (2018a) describe a parallel programme of cyclic testing at SNW that offered the first systematic study of how 'virgin' open driven steel piles respond to repetitive tension loading in chalk. Experiments were conducted on seven fully aged, 139 mm outside diameter (D) un-instrumented steel tubular 'SD' piles driven above the water table to 5·5 m tip depths (L_p) giving $L_p/D \approx 40$. The piles had ≈ 9 mm wall thicknesses (t_w) and $D/t_w \approx 15{\cdot}4$. Static reference tests on control piles confirmed that monotonic capacity developed after ≈ 250 days of ageing after driving and identified the reference static tension capacities available prior to applying up to 1000 cycles.

The most severe one-way tension cycling led to unstable (US) outcomes when the 'static factors of safety' (FoS) defined as Q_{max}, the maximum cyclic tension load, divided into Q_{ref}, the static reference tension capacity, fell below $\approx 1{\cdot}45$. Pile displacements accumulated rapidly, axial stiffnesses fell, and failures developed with $N < 100$. Piles subjected to one-way cyclic loading with $1{\cdot}45 < \text{FoS} < 2{\cdot}1$ remained un-failed after 1000 cycles. Their displacements accumulated broadly in proportion to $N^{0{\cdot}33}$ for the limited range of conditions considered. Test outcomes were classified as being either stable (S) or meta-stable (MS) according to their displacement and the capacity trends proven by post-cyclic static tests: cycling could either improve or degrade axial capacity.

Buckley *et al*. (2018a) were not able to explore either two-way cycling, which was expected to lead to more marked cyclic degradation, or the response of piles with larger diameter. Both issues were considered critical to practical application.

The ALPACA programme

The ALPACA (axial–lateral pile analysis for chalk applying multi-scale field and laboratory testing) and ALPACA-Plus joint industry research projects (JIPs) outlined by Jardine *et al*. (2019) tackled the axial and lateral dynamic, cyclic and monotonic behaviour of mostly tubular steel piles with diameters ranging from 139 mm to 1·8 m. Over 40 piles were driven at SNW between 2017 and October 2020 to depths both above and well below the water table. Most were equipped with strings of closely spaced fibre-optic strain gauges; Jardine *et al*. (2023) report the site layout and identify the piles assigned to phased monotonic and cyclic, axial and lateral testing between May 2018 and December 2021.

Outcomes from ALPACA monotonic axial experiments

Twenty-two 'virgin' corrodible steel piles were subjected to monotonic axial testing. Four stainless steel and concrete piles were driven and tested to isolate the potential impact of corrosion processes. Jardine *et al*. (2023) describe how pore-pressure dissipation, effective stress re-distribution and long-term corrosion processes control axial set-up and led to quite different ageing trends above and below the water table. Other key observations include: (*a*) the Chalk ICP-18 approach provided good predictions for driving resistances; (*b*) long-term compression shaft capacity is around double that available in tension, as reported at other chalk sites by Vinck (2021); (*c*) long-term local shaft stresses decline more sharply with h/R than expected by Chalk ICP-18; (*d*) closed piles develop far higher capacities than open-ended equivalents; and (*e*) base capacities also show some set-up. Jardine *et al*. (2023) applied these findings in a comprehensive recalibration of Chalk ICP-18.

ALPACA AXIAL CYCLIC PROGRAMME

This paper reports the ALPACA one-way tension and two-way (compression and tension) testing on 14 'virgin' open steel 139 and 508 mm D piles, supported by monotonic control tests, integrating their outcomes with the Buckley *et al*. (2018a) study. Noting that open tubular driven piles develop far higher compressive than tensile shaft capacities in chalk and that cyclic tension cases are the most critical for lightweight offshore wind turbines (Barbosa *et al*., 2017), the programme focused on conditions where the loading was more onerous in tension than in compression. All the pile movements induced by cycling were consequently vertically upwards.

Test ground conditions

Principally CIRIA grade B2 (Lord *et al*., 2002) structured, very weak-to-weak, low-to-medium-density white chalk extends to well below the test pile tips. The chalk has a high degree of saturation above the water table, which is located at $\approx 0{\cdot}9$ m $\pm$ 0·25 m above ordnance datum (AOD) at around 6 m below ground level. Closed-to-slightly-open stained joints and beds of 250 mm average thickness, along with systems of micro-fissures, provide pathways for air above the water table and water below it.

Monotonic and cyclic behaviour of SNW chalk

Vinck *et al*. (2022) describe the intensive characterisation conducted for ALPACA through in situ profiling and laboratory testing on high-quality block and Geobore-S rotary samples. Liu *et al*. (2023) report additional triaxial tests involving effective cell pressures up to 12·8 MPa that modelled the conditions beneath the pile tips during driving and compression load testing, where local mean effective stresses as high as 10 MPa can develop (Jardine *et al*., 2023). The intact chalk starts to de-structure beneath the advancing tips and soft putty forms around the pile shafts in annuli, which have similar thicknesses to the pile walls. The de-structured annuli reconsolidate after driving and Jardine *et al*. (2023) conclude that their properties and states control the aged piles' axial resistances. Liu *et al*. (2022) report monotonic and cyclic triaxial tests on de-structured chalk that matched the putty conditions, showing that its behaviour is silt-like. The de-structured putty shows modest cyclic resistances that are governed by the applied consolidation stresses. Its cyclic failure involves sharp pore pressure build-up, leftward drifting of the effective stress paths, cyclic stiffness losses and growing damping ratios. Liu *et al*. (2022) established normalised relationships between cyclic loading parameters, mean effective stress drifts $\Delta p'/p'_0$ and strain development from their main test series on specimens consolidated (isotropically) to 200 kPa. They also noted that samples consolidated to 400 kPa developed slightly higher drift and strain rates under comparable normalised cyclic loading levels. As discussed later, more marked leftward effective stress path drifting is anticipated under simple shear conditions, and alongside pile shafts, than is seen in triaxial tests.

The surrounding intact chalk provides stiff radial containment to the reconsolidated putty annuli formed around the pile shafts and constrains any dilation that develops as the putty fails monotonically or degrades under cycling. Ahmadi-Naghadeh *et al*. (2022) investigated intact SNW chalk's undrained cyclic triaxial behaviour under in situ stress conditions. High-quality samples could withstand one-way deviator stress amplitudes, $q_{cyc} = \Delta\sigma_1 - \Delta\sigma_3$, up to 700 kPa in a fully stable manner. In cases where failure developed under higher-level cycling, the intact chalk's cyclic response remained stiff, with little or no sign of pore pressure change or impending instability until shortly

Downloaded by [] on [30/05/24]. Published with permission by the ICE under the CC-BY license

before abrupt brittle failure. Although chalk can be reduced to putty by high-level repetitive straining, its response to one-way, stress-controlled cycling resembles that of rocks, concrete or metals.

Pile arrangements and instrumentation

Aiming to check for any potential effects of scale on cyclic response, ALPACA employed a wide range of pile diameters and ages after driving. Table 1 summarises the axial–cyclic subset of eight nominally identical 508 mm D open tubular 'LD' piles driven to 10·15 m tip depths, with 41% of their shaft lengths below the water table and $L_p/D \approx 20$. The piles' 20·6 mm wall thicknesses (giving relatively low $D/t_w \approx 25$) were instrumented with opposing strings of optical fibre Bragg grating (FBG) strain gauges (Buckley *et al.*, 2020b). Axial–cyclic tests were also conducted on six new 'SD series' 139 mm D piles, one of which also carried FBG gauges. These piles terminated above the water table at $5{\cdot}45 \pm 0{\cdot}1$ mbgl depths.

The test piles' average end of driving (implicitly compressive) unit shaft resistances of ≈ 20 to ≈ 32 kPa, as computed with the aid of iterative signal matching analyses, fell systematically with L_p/D due to the 'h/R' (or more loosely 'friction fatigue') processes outlined by Jardine *et al.* (2023). All were left undisturbed for 7 to 11 months before applying any loading. Static tension 'control' tests were conducted on three further LD and SD piles to define average reference static tensile shaft capacities Q_{ref} under conditions that matched the ages of the cyclic test piles. The shaft capacities were corrected for the piles' and chalk plugs' effective self-weights. The brittle and free-draining nature of the chalk eliminated the need to discount any reverse end-bearing resistances. The average tensile shaft resistance τ_{avg} plotted against normalised axial displacement (w/D) trends from the control piles' slow, stage-loaded, monotonic tension tests, including the 'SD' case of Buckley *et al.* (2018a) are shown in Fig. 1. Differences of ±15% in shaft capacity were found between similar (relatively slow) maintained load tests on the piles, which may reflect local variations in ground profile, pile surface conditions, installation details, test ages or load step choices (Jardine *et al.*, 2023). The SD piles' higher peak τ_{avg} and w/D ratios at failure reflect the higher degrees of set-up Λ that developed above the water table through air-enhanced corrosion processes. The average unit shaft resistance measured in a parallel compression test on an LD pile was $\approx 2{\cdot}1$ that in tension, which in turn was $\approx 1{\cdot}9$ times the 20 kPa default CIRIA design recommendation given by Lord *et al.* (2002).

Cyclic testing sequence

Axial cyclic loading was applied 224 to 256 days after driving for the LD piles and after 327 to 332 days for the SD cases. One-way tension cyclic loading (axial one-way cyclic loading (A1W)) tests reacted against steel and timber foundation pads. Two-way (axial two-way cyclic loading (A2W)) tests, that applied both compression and tension loads, reacted against kentledge and adjacent piles, respectively, in the SD and LD tests. None of the tests applied a significantly compressive mean load. Four displacement transducers placed equally around the pile axes measured axial movements relative to reference frames fixed to sufficiently distant datum points. Strain gauged load cells measured the constant-amplitude sinusoidal loading applied through automated hydraulic systems at $\approx 0{\cdot}1$ Hz, the frequency routinely adopted to match offshore wave loading (e.g. Lombardi *et al.*, 2017).

The tests applied sinusoidal load cycles, as defined in Tables 2 and 3, where Q_{cyc} is the (half peak-to-trough) load amplitude and Q_{mean} is the mid-cycle value. Both are normalised by the listed Q_{ref} values from the monotonic tension tests. Cycling continued until either failure occurred after N_f cycles, or the pre-programmed (typically 1000 to 2000 cycles) test durations were reached without any failure. One test extended to 10 000 cycles to check longer-term trends. All started with an initial batch of cycles that was designed to avoid failure. Around half the piles were subjected to a distinctly higher-level second cyclic batch after allowing a short pause. For the LD tests, these pauses typically extended for the 20 to 40 min required to re-set the loading system, while only 3 to 5 min delays were required for the SD piles. The potential impact of stable initial cyclic loading on any far higher-level second batch was assumed negligible. Final stage loaded axial static tension (AST) tests to failure were conducted on all piles, typically within around 2 h of their final cycle. Working day limitations led to shorter maintained load 'creep' stages being imposed than in the reference tests. Loads, displacements and FBG strains were recorded throughout each cycle of loading; a logging malfunction led to displacement data being lost over the first 1000 cycles of test S20.

Failure and stability criteria

As outlined below, the cyclic test outcomes fell into three categories following a scheme modified slightly from those employed previously (Karlsrud *et al.*, 1986; Poulos, 1988; Jardine & Standing, 2012; Buckley *et al.*, 2018a). The same normalised criteria were applied to the LD and SD tests and,

Table 1. Test pile geometries for tubular steel piles tested under axial cyclic loading

Test	Date tested	Age: days	Pile type	D: m	D/t_w	L/D	Type
5	3 July 2018	224	LD11-A1W	0·508	25	20	First time axial one-way cyclic
6	5 July 2018	226	LD02-A1W	0·508	25	20	First time axial one-way cyclic
7	13 July 2018	234	LD10-A2W	0·508	25	20	First time axial two-way cyclic
8	18 July 2018	239	LD08-A1/2W	0·508	25	20	First time axial one-/two-way cyclic
10	23 July 2018	243	LD03-A1W	0·508	25	20	First time axial one-way cyclic
11	25 July 2018	246	LD04-A1W	0·508	25	20	Extended 10 000 cycle test
12	1 August 2018	252	LD01-A1/2W	0·508	25	20	First time axial one-/two-way cyclic
13	4 August 2018	256	LD09-A1/2W	0·508	25	20	First time axial one-/two-way cyclic
S20	6 April 2019	327	SD06-A2W	0·139	15	39	First time axial two-way cyclic
S21	8 April 2019	329	SD04-A2W	0·139	15	39	First time axial two-way cyclic
S22	8 April 2019	329	SD03-A1W	0·139	14	40	First time axial one-way cyclic
S23	9 April 2019	329	SD11-A2W	0·139	14	38	First time axial two-way cyclic
S25	10 April 2019	331	SD02-A1W	0·139	15	39	First time axial one-way cyclic
S27	11 April 2019	332	SD01-A1W	0·139	15	40	First time axial one-way cyclic

A1W, axial one-way cyclic; A2W, axial two-way cyclic.

Downloaded by [] on [30/05/24]. Published with permission by the ICE under the CC-BY license

as all displacements were vertically upwards, the pile loads are normalised by the tension shaft capacity applying prior to cycling.

Unstable (US). Failure occurs within 1000 cycles after marked reductions in shaft capacity and pile loading stiffness k_L. The axial movements required to reach failure in slow monotonic maintained tension load tests were relatively small (0·02 to 0·04D) for most ALPACA piles (Jardine *et al.*, 2023). Noting that generally smaller displacements could be expected in faster 0·1 Hz cyclic tests, the onset of cyclic failure was defined as the point where either the accumulated peak displacement, a, reached 0·02D or the peak-to-trough displacements, d_a, exceeded 0·01D, as defined, with cyclic stiffness, in Fig. 2. The accumulated peak displacement criterion was usually the most critical, although peak-to-trough movements became more important in tests with low mean loads and high cyclic amplitudes.

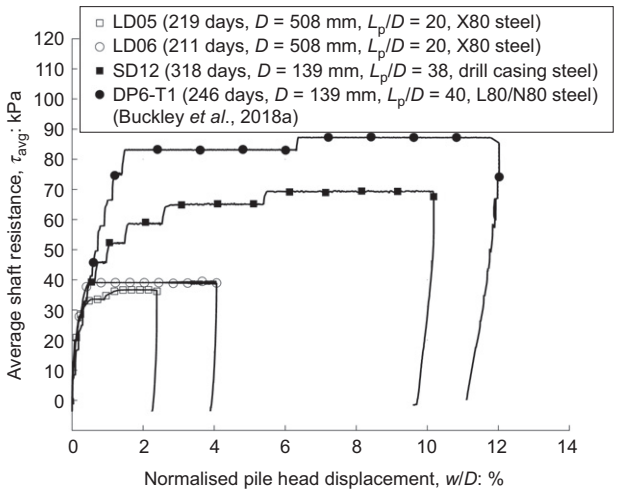


Fig. 1. Trends for average tensile shaft resistance for the reference LD and SD pile tests

Stable (S). Shaft capacity does not degrade significantly and accumulated total displacements remain negligibly small over at least 1000 cycles. 'Negligible' is taken here to mean no more than one-tenth of the accumulated peak and peak-to-trough displacements associated with failure, or 0·002D and 0·001D, respectively. Stable cycling can lead to tension capacities increasing marginally while peak-to-trough movements can reduce, leading to increasing pile stiffnesses.

Metastable (MS). These are cases that fall between these limits. Piles do not fail within 1000 cycles, but accumulated displacements may exceed 0·002D and/or peak-to-trough displacements exceed 0·001D. Tension capacity and pile stiffness reductions may occur, but insufficiently for the failure criteria to be met within 1000 cycles.

It is often acceptable in practice to design a foundation to sustain limited numbers of metastable loading cycles,

Table 2. Axial cyclic tests on LD piles

Test	Pile type	Q_{ref}*: kN	Q_{min}†: kN	Q_{max}†: kN	Q_{mean}/Q_{ref}	Q_{cyc}/Q_{ref}	Q_{max}/Q_{ref}	N	N_f	Class	Q_{pc}/Q_{ref}
5	LD11-A1W	620	71	276	0·28	0·17	0·44	2000	—	S	1·01
6	LD02-A1W	620	0	389	0·31	0·31	0·63	2000	—	MS	0·89
7	LD10-A2W	620	−61	19	−0·03	0·06	0·03	1000	—	S	—
7A	LD10-A2W	620	−268	339	0·06	0·49	0·55	283	256	US	0·41
8	LD08-A1W	620	81	223	0·24	0·11	0·36	2000	—	S	—
8A	LD08-A2W	620	−161	449	0·23	0·49	0·49	21	13	US	0·39
10	LD03-A1W	620	316	452	0·62	0·11	0·73	1000	—	S	—
10A	LD03-A1W	620	5	455	0·37	0·36	0·73	1000	—	S	1·65
11	LD04-A1W	620	181	455	0·51	0·22	0·73	10 000	—	S	1·10
12	LD01-A1W	620	201	341	0·44	0·11	0·55	1000	—	S	—
12A	LD01-A2W	620	−218	236	0·01	0·37	0·38	1000	—	MS	0·83
13	LD09-A1W	620	402	542	0·76	0·11	0·87	1000	—	MS	—
13A	LD09-A2W	620	−111	343	0·19	0·37	0·55	69	56	US	0·78

*Q_{ref} taken as average of static axial capacities on first time axial tension tests (test 1 and test 3 at 211 and 219 days, respectively; see Jardine *et al.* (2023)).
†Actual applied loads accounted for weight of steel and chalk plug.

Table 3. Axial cyclic tests on SD piles

Test	Pile type	Q_{ref}: kN	Q_{max}*: kN	Q_{min}*: kN	Q_{mean}/Q_{ref}	Q_{cyc}/Q_{ref}	Q_{max}/Q_{ref}	N	N_f	Class	Q_{pc}/Q_{ref}
S20†	SD06-A2W	162	16	−16	0·00	0·10	0·10	1500†	—	S	—
S20A	SD06-A2W	162	66	−66	0·00	0·41	0·41	45	25	US	0·62
S21	SD04-A2W	162	70	−34·1	0·11	0·32	0·43	55	32	US	0·56
S22	SD03-A1W	162	108	76	0·57	0·10	0·67	1000	61	US	0·76
S23‡	SD11-A2W	162	34	2	0·11	0·10	0·21	1720	—	—	—
S23A	SD11-A2W	162	70	−34	0·11	0·32	0·43	49	11	US	0·62
S25	SD02-A1W	162	66	17	0·26	0·15	0·41	1066	—	MS	—
S25A	SD02-A1W	162	102	7	0·34	0·29	0·63	1008	—	MS	1·06
S27	SD01-A1W	162	81	49	0·40	0·10	0·50	1062	—	MS	—
S27A	SD01-A1W	162	107	39	0·45	0·21	0·66	1002	471	US	0·87

*Actual applied load accounted for weight of steel and chalk plug.
†One thousand unlogged cycles applied prior to test S20.
‡Loads not achieved consistently in test S23 – results not used.

Downloaded by [] on [30/05/24]. Published with permission by the ICE under the CC-BY license

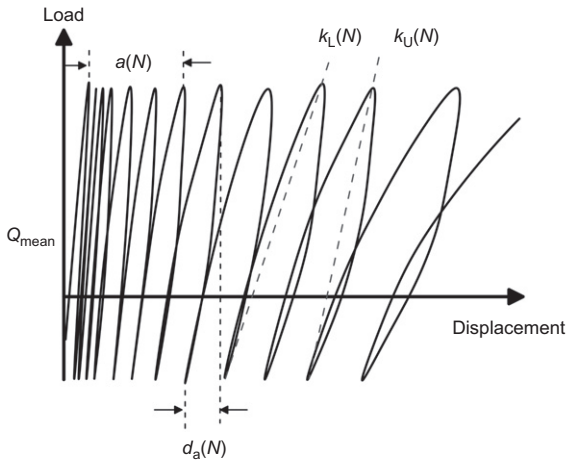


Fig. 2. Schematic illustration of cyclic displacement and stiffness parameters

provided that appropriate factors are applied to ensure that the piles satisfy the safety and serviceability criteria applying under the site-specific cyclic design conditions; see, for example, Jardine *et al.* (2012).

Adopting displacement-based criteria in addition to those related to axial capacity trends allowed the test outcomes to be categorised, including 'first-stage' tests that did not conclude with tension loading to failure. Naturally, applying different criteria to those outlined above could lead to individual tests falling into different categories.

RESULTS AND INTERPRETATION

The cyclic tests' loading conditions are plotted in Fig. 3 in normalised interaction diagrams that also indicate the total number of cycles, N, applied. As noted earlier, the undisturbed tension capacities of individual cyclic test piles may differ from the reference values and the true test coordinates could vary up to ±15% from those plotted. Corrosion processes were identified by Jardine *et al.* (2022) as being important to pile capacity gains over time (or 'set-up') at SNW and responsible for higher pre-loading local radial (σ'_{rc}) stresses applying in the de-structured chalk around their shafts, as well as potentially boosting the 'constrained dilation' $\Delta\sigma'_{rd}$ increases that have been proven to develop on loading in chalk (Buckley *et al.*, 2018b). Their contribution to overall shaft capacity is known to vary inversely with pile diameter (Jardine *et al.*, 2018).

All the pile tests involved upward movement trends and those annotated as F underwent tension shaft failures after N_f cycles. The top left to right bottom diagonals represent lines of static FoS = Q_{ref}/Q_{max}. Tentative $N_f = 10$, 100 and 1000 contours are plotted to indicate the normalised cyclic load combinations under which the specified numbers of cycles are required to reach failure. All contours must converge to $Q_{cyc}/Q_{ref} = 0$ when $Q_{mean}/Q_{ref} = 1$, the point which represents monotonic failure. By definition, all loading conditions plotting above the $N_f = 1000$ contours should be unstable (US) and those below are either metastable (MS) or stable (S). However, the implicit ±15% scatter in monotonic capacity and the potential impacts of variations in individual testing conditions made it difficult to find contours that fit all outcomes fully satisfactorily. The safety implications of underestimating cyclic impact led to choosing contours on a marginally 'conservative', rather than a best fit, basis. Among the LD tests, one failed at an N value lower than implied by the nearest contour, while three that ended

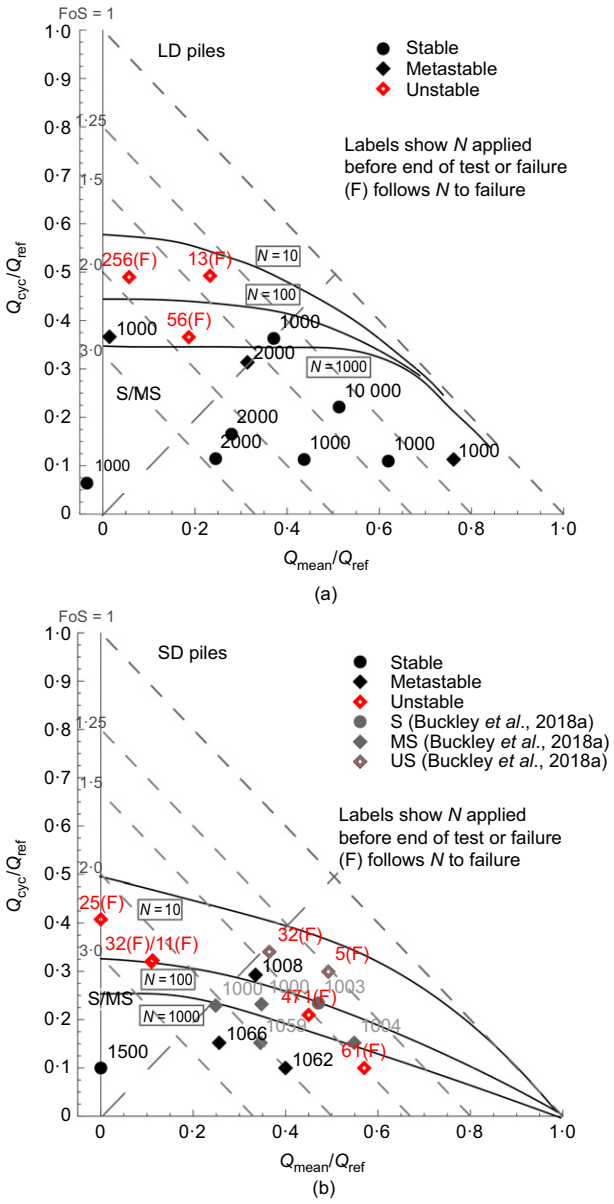


Fig. 3. Cyclic loading interaction diagrams with numbers of cycles to the end of the test or failure: (a) LD tests; (b) SD tests from this study and from Buckley *et al.* (2018a)

without failure plotted 'conservatively' above the $N = 100$ or $N = 1000$ failure contours. The SD series included two tests that failed at N values lower than implied by their nearest contour failure contours, while five un-failed tests plot 'conservatively' on or above the $N = 100$ or $N = 1000$ contours. The scales of the outlying SD and LD tests' deviations from the expected overall contour system were generally less than ±0·1 Q_{ref}.

The LD tests' contours shown in Fig. 3(a) plot, on their left-hand sides, up to 0·12 above their SD equivalents in Fig. 3(b). As noted earlier, the SD piles developed ≈80% higher 'aged' unit shaft resistances, mainly due to corrosion-linked processes being more active above the water table. SD piles could only survive 1000 one-way cycles (imposing $Q_{mean} = Q_{ref}$) when the ratio of monotonic shaft capacity to maximum cyclic load (or FoS) exceeded ≈1·6, while the LD piles survived all one-way cycling. Model tests reported by Tsuha *et al.* (2012) show that the 'constrained dilation' $\Delta\sigma'_{rd}$ radial stress component is less effective in resisting cyclic loading in sand, so the lower cycling resistance of the SD

Downloaded by [] on [30/05/24]. Published with permission by the ICE under the CC-BY license

piles may reflect an associated effect of scale. The contours confirm that far higher 'static' FoS values are required to survive extreme two-way cycling than under any one-way condition: SD piles could only survive 1000 symmetrical two-way cycles (with $Q_{mean}/Q_{ref} \approx 0$) if FoS > 3·6, while the equivalent LD tests remained un-failed when FoS > 2·9. Comparable FoS limits were interpreted from cyclic tests on 457 mm D steel pipe piles driven in dense sand at Dunkirk, France (Jardine & Standing, 2012).

Impact on overall and local shaft tension capacity

The ALPACA tests' ratios of post-cyclic capacity, Q_{pc}, to monotonic reference tension capacity are listed in Tables 2 and 3. Allowing for test pile variability, the 'unfailed' stable cases (tests 5, 10A, 11) suffered little or no degradation. Their average Q_{pc}/Q_{ref} ratio (1·25) indicates capacity gains, as noted in Dunkirk sand by Jardine & Standing (2012). Metastable loading (in tests 6, 12A and S25A) led to marginal degradation and an average of 0·93. The unstable piles' ratios ranged from 0·39 to 0·87, with an average ≈ 0·63. Failure occurs when shaft capacities degrade to match the applied Q_{max}. The unstable piles' post-test capacities scattered around an average $Q_{pc}/Q_{max} \approx 1{\cdot}07$, possibly reflecting marginal recovery over the ≈ 2 h that typically elapsed between the final cycle and reaching peak capacity stages of check tests.

Further insights are given into shaft capacity degradation by the dual strings of FBG strain gauges installed on all LD piles. Careful analysis and filtering allowed axial pile load–depth profiles to be established for all test stages. Differentiation with respect to depth identified the shaft shear stresses transferred to the chalk. Any degradation under cycling can be identified by comparing the limiting tension profiles from (*a*) the end-of-driving (EoD) profiles established from back-analysis of fully instrumented dynamic tests, tentatively divided by 2 to predict EoD tension resistance; (*b*) the 'aged reference' tension test; (*c*) peak tension loading over the second ($N = 2$) cycle; and (*d*) the post-cyclic monotonic tension test conducted after the batch of cycling.

The profiles for test 11, which was fully stable over 10 000 cycles, are presented in Fig. 4(a). The $N = 2$ peak cyclic loading profile remained largely below the reference static test curve and the post-cycling profile confirms marginal capacity enhancement. However, unstable cases, such as tests 8A and 13A illustrated in Figs 4(b) and 4(c), manifested markedly reduced shaft capacity from the reference static test curve after 21 and 69 cycles, respectively. In both cases degradation was greatest over the lowest shaft sections where the reference static resistances were highest because the de-structuration that occurs during driving increases systematically with normalised distance (h/R) above the pile tip (Jardine *et al.*, 2018, 2023; Buckley *et al.*, 2020a). Comparison with the EoD profiles (corrected to tension resistances) reported by Jardine *et al.* (2023) shows that cycling to failure reduces local resistances at points within 1 to 2 m of the pile tip to below the EoD values but induces less damage higher on the shaft. The uppermost 2 m, where access to air accelerated corrosion and set-up, was also degraded markedly in test 08A. Top-down patterns of cyclic degradation are more common with other geomaterials (see Erbrich *et al.* (2010) or Jardine *et al.* (2012)). The LD and SD piles had relatively high axial stiffness due to their relatively low D/t_w ratios; a more top-down degradation pattern might apply to piles driven with higher D/t_w or L/D ratios.

Styles of load–displacement response

The tests' load–displacement responses reflect their degrees of cyclic stability. The long-term stable test 11, illustrated in Fig. 5, developed just 1 mm of accumulated peak displacement over 10 000 cycles, while the unstable

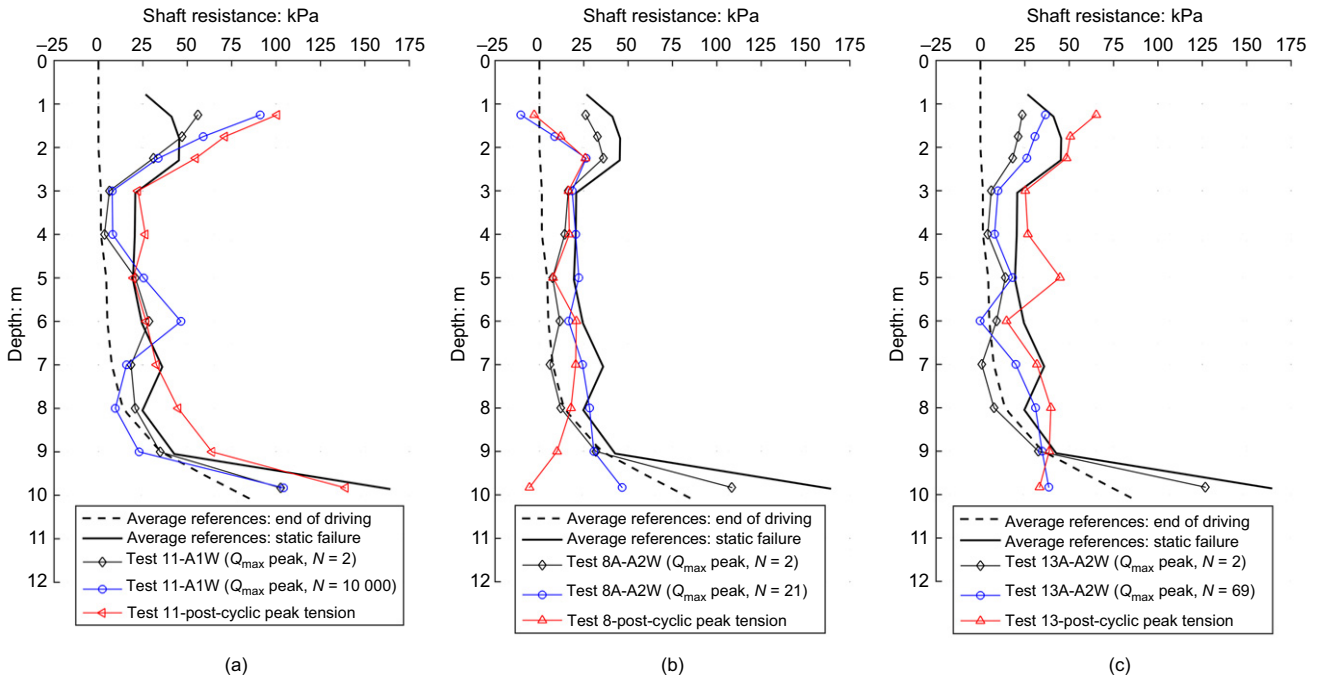


Fig. 4. (a) Local shaft shear stresses evaluated from peak tension loading stage of stable test 11 A1W, at the beginning of cycling ($N = 2$), after 10 000 cycles and post-cyclic tension loading to failure. Profiles of shaft resistance at end of driving (EoD) and static tension failure averaged from the two reference tests are also shown, divided by 2 to indicate EoD tension resistances. (b) Local shaft shear stresses evaluated from peak tension loading stage of unstable test 8A A2W, at the beginning ($N = 2$) and end ($N = 21$) of cycling, and post-cyclic tension loading to failure. Profiles of shaft resistance at EoD and static tension failure averaged from the two reference tests are also shown divided by 2 to indicate EoD tension resistances. (c) Local shaft shear stresses evaluated from peak tension loading stage of unstable test 13A A2W, at the beginning ($N = 2$) and end ($N = 69$) of cycling, and post-cyclic tension loading to failure. Profiles of shaft resistance at EoD and static tension failure averaged from the two reference tests are also shown, divided by 2 to indicate EoD tension resistances

Downloaded by [] on [30/05/24]. Published with permission by the ICE under the CC-BY license

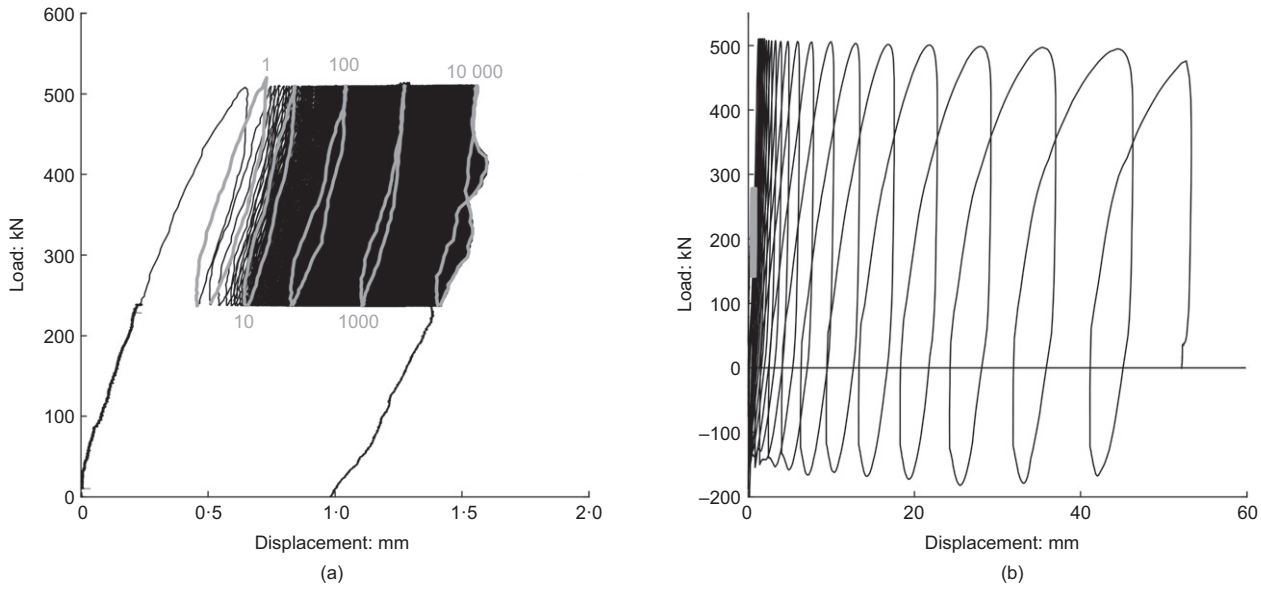


Fig. 5. Example load displacement response during: (a) stable extended cycle A1W test 11 on LD04; (b) unstable A2W test 8A on LD08

loading applied to a similar pile in test 8A developed large movements as it progressed to fail within 11 cycles. Figs 6–8 plot the normalised absolute and double-amplitude displacement accumulation trends with the number of cycles N for all tests, grouping the unstable (US), metastable (MS) and stable (S) cases into sub-sets. The US tests displayed the most variation, with some failing over their first few cycles, while others accumulated displacements more slowly. Some showed marked upward inflections towards abrupt failures, while others crept towards gentle failures over several hundred cycles.

The MS category showed more systematic trends with the double-amplitude displacements, and the rates of total displacement accumulation, declining systematically with N. Finally, the stable (S) tests showed only modest displacement accumulation over their first few hundred cycles, as observed by Buckley *et al*. (2018a).

Trends in accumulation of cyclic displacement

It is argued in the Appendix that any accumulated peak cyclic pile head displacements are dominantly generated by plastic shear straining within the annular zone of putty chalk that forms around the pile during driving. Noting that the widths of the putty zones are practically equal to the pile wall thickness, t_w (see Buckley *et al*. (2018a)), the absolute magnitudes of the accumulated peak pile head displacements, a, are expected to scale linearly with t_w when all loading factors are held constant. Logarithmic plots of the stable and metastable tests' absolute cyclic displacements (defined in Fig. 2) trends reveal power law trends with N of the form

$$\frac{a}{t_w}(\%) = \frac{D}{t_w}\alpha N^{\beta} \tag{1}$$

where α and β are non-dimensional fitting parameters that vary with the normalised cyclic loading levels. Fig. 9 shows examples of the fitted power law trends for the MS and S classification tests, while Table 4 gives the best-fitting α and β values for individual tests.

Equations (2) and (3) were developed to relate α and β more generally to the normalised cyclic loading parameters through a global fitting approach that gave the least average absolute differences between the measured and predicted cyclic displacements developed after 10, 100 and 1000 cycles across the full set of metastable and stable tests on SD and LD piles, giving the average errors listed in Table 5. Parameter α was found to be largely independent of the cyclic loading ratio (Q_{cyc}/Q_{ref}), while parameter β was insensitive to the mean load level (Q_{mean}/Q_{ref}). However, as with the cyclic failure contour plots discussed above, scatter between test outcomes made it difficult to fit all tests satisfactorily. The overall best-fitting global expressions (equations (2) and (3)) gave 'good' fits to about 30% of cases, 'acceptable' matches to 50% and 'poor' fits to the remaining 20%.

$$\alpha = \frac{t_w}{D} \times \left(0{\cdot}95 \times \frac{Q_{mean}}{Q_{ref}} + 0{\cdot}0025\right)(\text{in } \%) \tag{2}$$

$$\beta = 1{\cdot}73 \times \frac{Q_{cyc}}{Q_{ref}} \tag{3}$$

Figure 10(a) presents examples of two 'good' fits, while Fig. 10(b) shows two 'poor' examples. These latter cases' variations from expected behaviour may be related to unknown variations in the piles' monotonic reference capacities and the cyclic test outcomes' sensitivity to the normalised cyclic loading parameters.

Axial cyclic stiffness trends

The cyclic tests' double-amplitude displacements led to global cyclic pile stiffnesses, k_L, as defined in Fig. 2 which reduced systematically with cyclic load amplitude and evolved as cycling progressed. Figs 11–13 present the stiffness trends, grouped by stability classification. The unstable tests generally showed clear, marked, stiffness reductions from the onset of cycling up to failure. However, two SD tests, S22 and S27A, that plot along the FoS = 1·5 line in Fig. 3, accumulated peak displacements more slowly than other unstable tests (see Fig. 6) and manifested relatively stable stiffness trends up to the onset of failure.

The metastable LD tests also tended to show significant reductions from the onset of cycling, while their SD equivalents indicated relatively stable, slightly increasing stiffness. The stable LD tests showed steady, or increasing, stiffnesses trends.

Downloaded by [] on [30/05/24]. Published with permission by the ICE under the CC-BY license

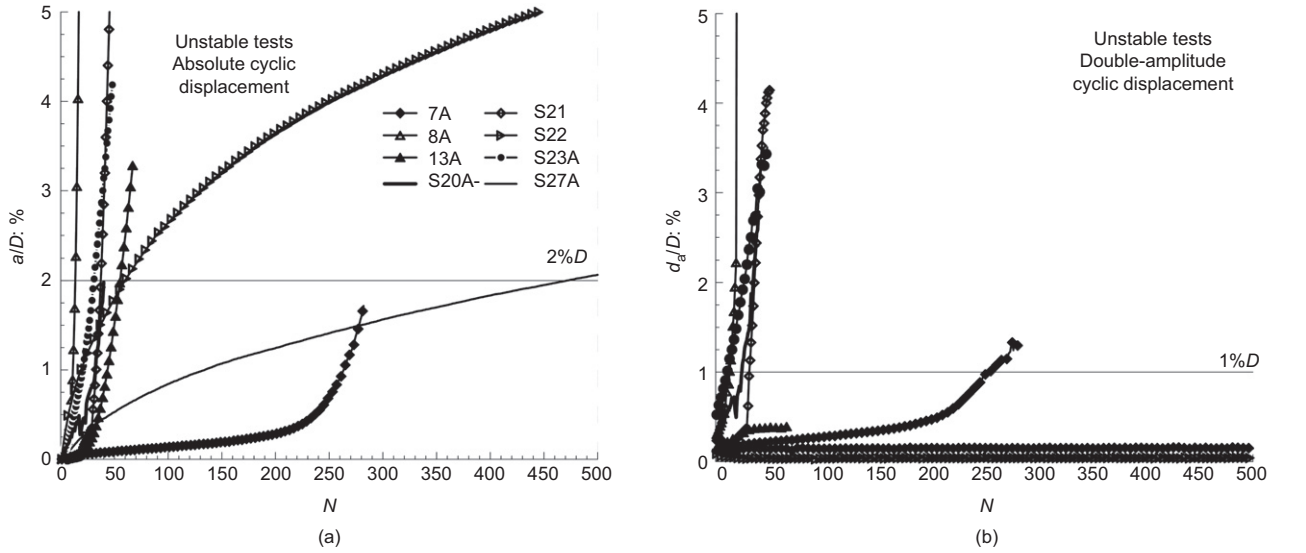


Fig. 6. Normalised displacement accumulation trends with cycling in unstable tests: (a) absolute displacement; (b) double-amplitude displacement

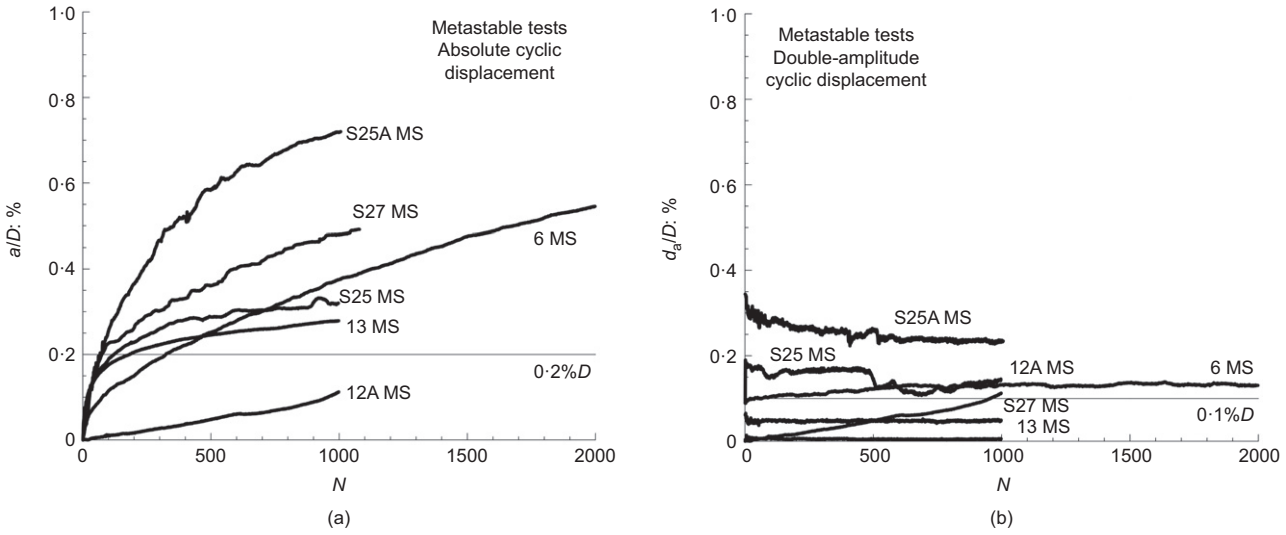


Fig. 7. Normalised displacement accumulation trends with cycling in metastable tests: (a) absolute displacement; (b) double-amplitude displacement

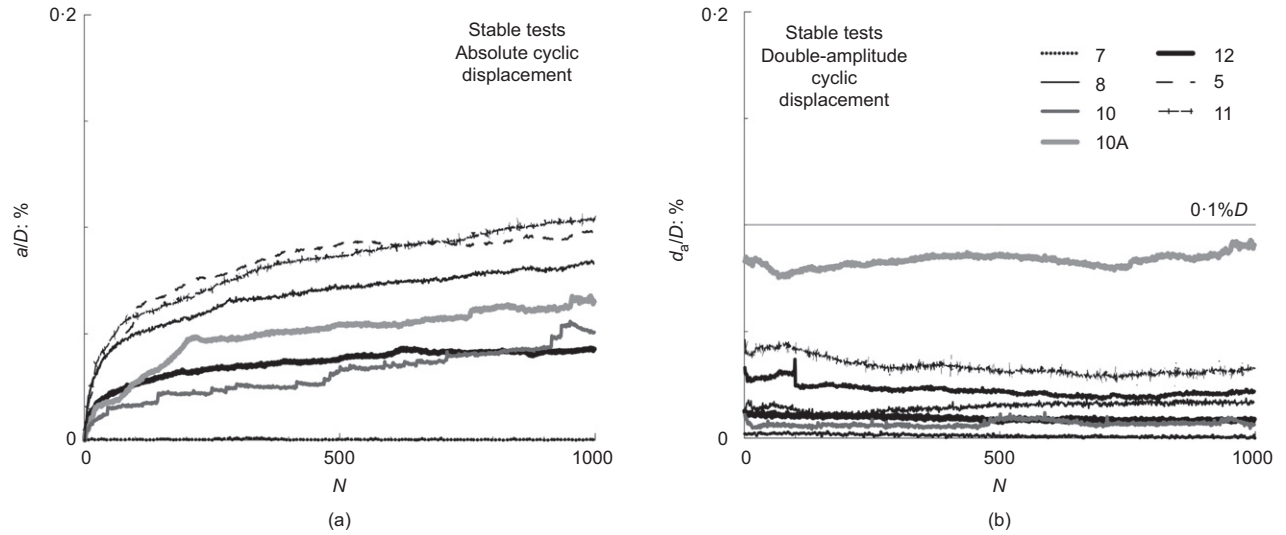


Fig. 8. Normalised displacement accumulation trends with cycling in stable/metastable tests: (a) absolute displacement; (b) double-amplitude displacement. S20 not shown due to missed cycles

Downloaded by [] on [30/05/24]. Published with permission by the ICE under the CC-BY license

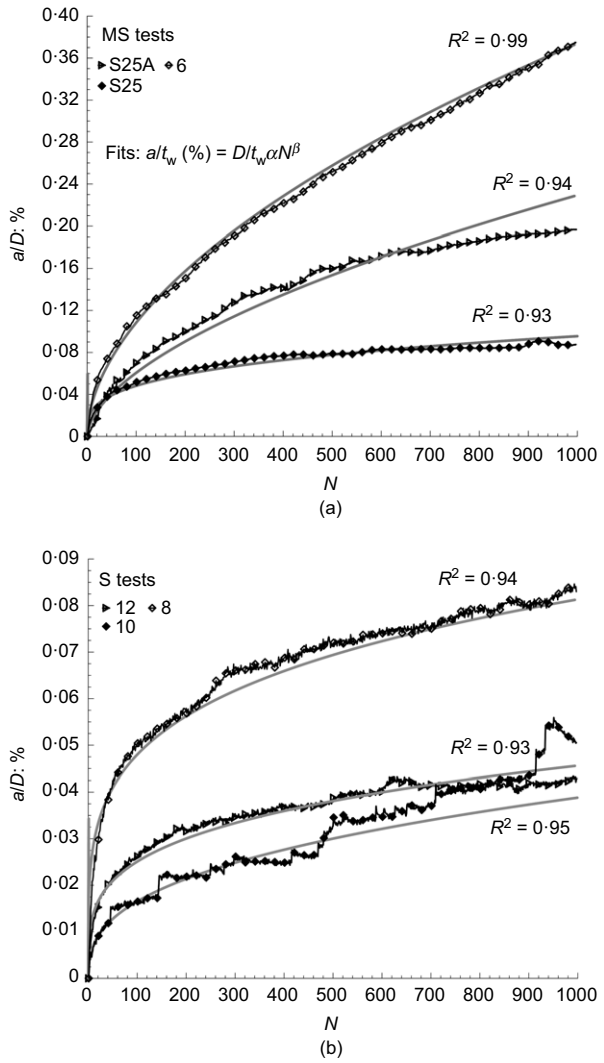


Fig. 9. Example power law fits to cyclic displacement trends: (a) metastable; (b) stable tests

Table 4. Cyclic loading parameters in stable/metastable tests

Test	Pile type	α: %	β	R^2	Class
5	LD11-A1W	0·0151	0·277	0·87	S
6	LD02-A1W	0·0091	0·538	1·00	MS
7*	LD10-A2W	—	—	—	—
8	LD08-A1W	0·0167	0·229	0·94	S
10	LD03-A1W	0·003	0·371	0·95	S
11	LD04-A1W	0·0183	0·248	0·92	S
12	LD01-A1W	0·0076	0·260	0·93	S
12A	LD01-A2W	0·0001	1·026	0·96	MS
13	LD09-A1W	0·0429	0·280	0·84	MS
S25	SD02-A1W	0·0449	0·296	0·93	MS
S25A	SD02-A1W	0·0154	0·58	0·94	MS
S27	SD01-A1W	0·0354	0·38	0·99	MS

*Actual absolute displacement $<0{\cdot}003\%D$.

The maximum k_L values observed in the cyclic tests were $\approx 6{\cdot}0 \times 10^5$ kN/m and $\approx 6{\cdot}0 \times 10^6$ kN/m for the SD and LD piles, respectively, after excluding the erratic trace from test 7. Jardine *et al.* (2023) report similar initial k values ($\approx 6{\cdot}0 \times 10^5$ kN/m and $\approx 2{\cdot}0 \times 10^6$ kN/m) from the earliest (near-linear) stages of the equivalent monotonic reference

Table 5. Average absolute differences between measured and predicted *a/D* (%) at three *N* levels from dataset

N	$N = 10$	$N = 100$	$N = 1000$
$\text{abs}[(a/D)_{pre} - (a/D)_{msd}]$	0·0194	0·0565	0·1194

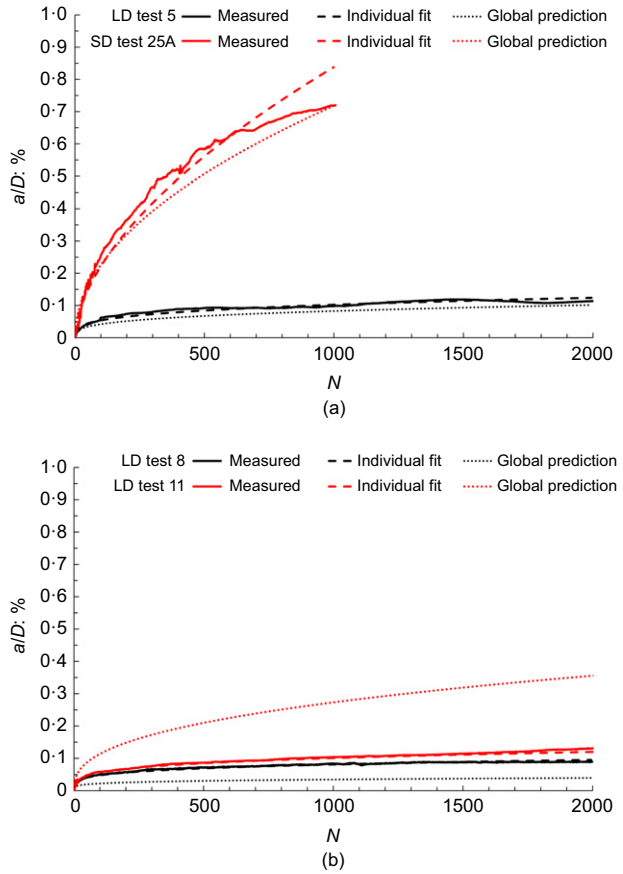


Fig. 10. Global prediction of absolute displacement trends calculated using equations (1)–(3): (a) example of good fits; (b) example of poor fits

tests. These stages were analysed applying closed-form elastic solutions developed by the authors, through an extension of Randolph & Wroth's (1978) methodology, to account for the LD and SD piles' geometries, axial compressibility and zero base load under tension loading. Maximum elastic chalk vertical shear stiffnesses G_{vh} of 310 to 450 MPa were interpreted from the SD and LD pile tests, which correspond, on average, to $\approx 25\%$ of the average G_{vh} from nearby seismic CPT profiling; see Vinck *et al.* (2021). Jardine *et al.* (2022) ascribe this feature to the chalk's natural fissuring and the damage inflicted by pile driving, including the formation of the putty annuli.

MODELLING OF CYCLIC SHAFT FAILURE CONDITIONS

Model calibration chamber experiments involving highly instrumented mini-ICP piles installed in pressurised sand masses reveal that their cyclic shaft capacity degradation involves radial effective stresses reducing under the highly kinematically constrained, near-constant-volume, conditions applying at the soil–pile interface (Tsuha *et al.*, 2012). Cyclic triaxial, simple shear or hollow cylinder apparatus (HCA) laboratory tests indicate how effective stresses may reduce,

Downloaded by [] on [30/05/24]. Published with permission by the ICE under the CC-BY license

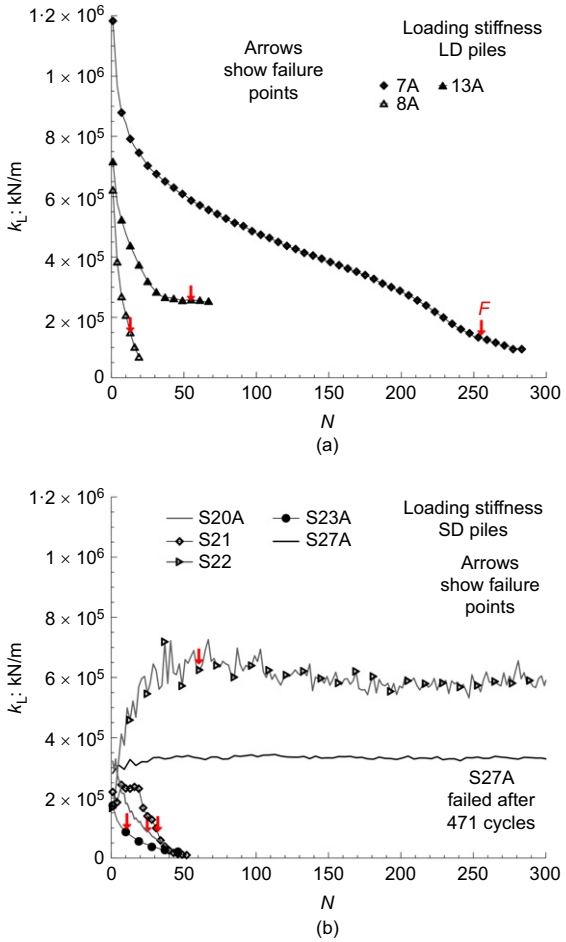


Fig. 11. Loading stiffness trends in unstable tests: (a) LD tests; (b) SD tests

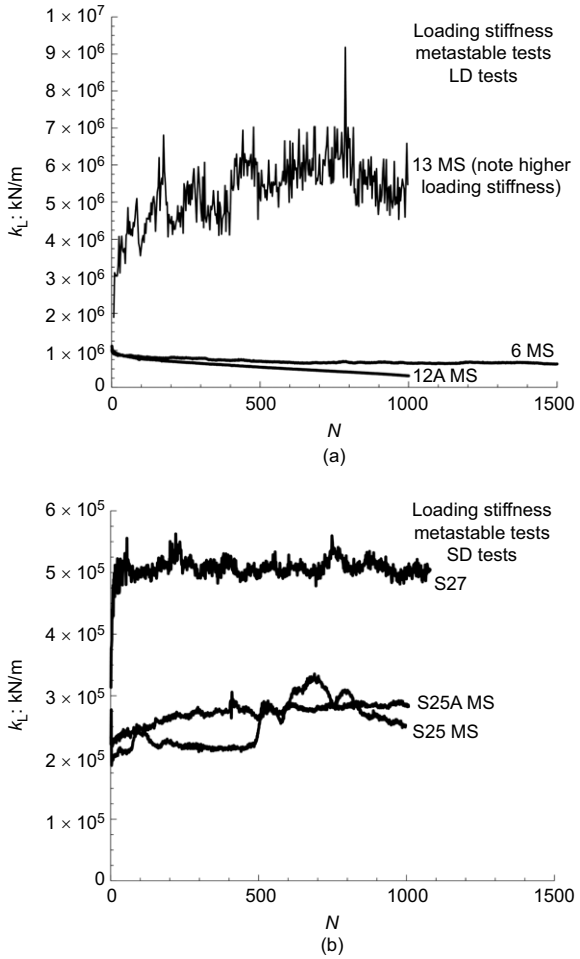


Fig. 12. Loading stiffness trends in metastable tests: (a) LD tests; (b) SD tests

permanent strains grow and stiffnesses fall as functions of the applied cyclic loading; see, for example, Aghakouchak (2015), Rattley *et al.* (2017) or Jardine (2020). While constant normal stiffness (CNS) tests may be attempted to model the pile shaft interface boundary conditions (Erbrich *et al.*, 2010), undrained laboratory tests also provide a representative and practical approach, especially when the surrounding soil mass is as stiff as the intact chalk.

Jardine *et al.* (2012) outline how cyclic laboratory tests may be applied in at least three ways to help predict pile stability under cyclic loading. The most theoretically attractive and yet challenging route is to employ fully-fledged numerical analyses employing cyclic constitutive models calibrated to the laboratory experiments. A second possible path involves conducting cyclic T–z analyses in which subsections of the pile are represented by local reaction models that degrade with cycling in accordance with the cyclic laboratory tests. Such an approach was applied by Atkins (2000) to model the Dunkirk sand cyclic tests successfully, while also offering scope to capture any progressive cyclic shaft failure as explored also by Erbrich *et al.* (2010) and others. However, a significant difficulty in applying such modelling is the 'bottom-up' rather than 'top-down' pattern of progressive failure pattern observed in the ALPACA field tests. Alternatively, a simplified global approach may be adopted that applies the laboratory tests uniformly over the whole pile. This implicitly neglects any progressive failure and gives no direct information on total displacements or stiffness. However, Aghakouchak (2015) and Jardine (2020) show that, when combined with suitably conditioned laboratory tests, the approach led to

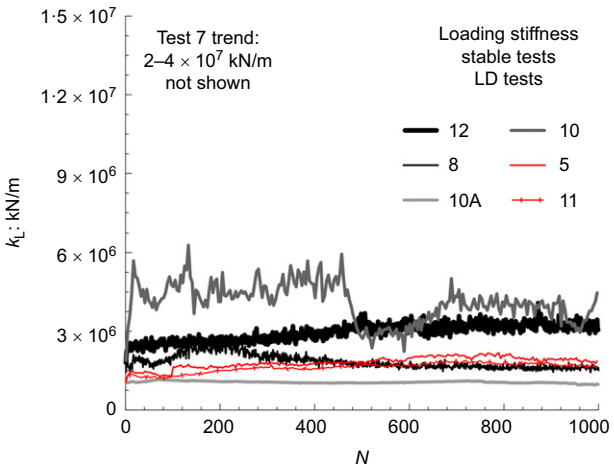


Fig. 13. Loading stiffness trends in stable tests

representative predictions for the failure conditions of cyclic field pile tests conducted at Dunkirk and model pile tests in NE34 sand. Rattley *et al.* (2017) further describe how a related approach allowed cyclic simple shear tests to be applied in cyclic design checks for a major offshore wind-farm. A similar simplified global approach is applied below to investigate the correspondence between the cyclic element testing and the cyclic failure of LD and SD piles under load-controlled field conditions.

Downloaded by [] on [30/05/24]. Published with permission by the ICE under the CC-BY license

The piles' axial capacities are controlled by the properties of, and conditions within, the reconsolidated de-structured annuli which are located around the pile shafts and constrained by the stiff intact chalk. Liu *et al.* (2022) explored how mean effective stresses decline under undrained cyclic loading within the de-structured annuli. Their main triaxial programme was run on samples isotropically reconsolidated to 200 kPa with further specimens consolidated to 400 kPa. Parallel monotonic tests indicated that the putty developed pre-phase transformation peak shear strengths $S_u^{\text{pre-PT}} = 0{\cdot}25p_0'$, so the two programmes considered conditions where the maximum shear stresses developed would be no greater than 50 and 100 kPa, respectively, matching the average monotonic shaft resistances of the LD and SD piles shown in Fig. 1, although subject to the local variations with depth illustrated in Fig. 4.

Predictions of the pile cyclic loading conditions at which failure would be reached after specified numbers of cycles were made from the cyclic triaxial test outcomes. The Appendix details how average degrees of shaft degradation were assessed following the procedures of Aghakouchak (2015) and Jardine (2020), adopting an interface failure angle $\delta_f' = 32°$ after ring shear tests by Vinck (2021) on de-structured chalk. The results are summarised in Fig. 14 by comparing the predicted 'global' contours for failures with $N_f = 10$, 100 and 1000 with the 'consciously conservative' contours taken from Fig. 3. The LD field test contours and those predicted from the $p_0' = 200$ kPa triaxial tests follow broadly similar tends, although the latter overpredict the Q_{cyc}/Q_{ref} ratios at which cyclic failure occurs at given N_f values, with the largest difference (0·1) applying to the $N = 10$ contour covering extreme two-way cycling, while the Q_{cyc}/Q_{ref} contours for $N = 1000$ agree within 0·03. This may reflect the conservative interpretation of the field tests, the progressive failure that occurs from the pile tip upwards (see Figs 4(b) and 4(c)) or other simplifying assumptions made in the analysis. The SD field contours are compared in Fig. 14(b) with predictions made from the more cyclically susceptible $p_0' = 400$ kPa triaxial tests that best match the SD piles' average shaft radial effective stresses. Here too, broadly similar patterns were obtained with $A = -0{\cdot}05$ and $B = -0{\cdot}05$, where A and B are fitting parameters for the effective stress degradation (see Appendix), although the predicted contours plot up to 0·15 Q_{ref} above the conservative trends interpreted from the pile load tests. As discussed in the Appendix and demonstrated in Fig. 15, the prediction for the smaller diameter SD piles may be more affected by the simplifying assumptions made regarding the influence of the constrained dilation component of monotonic shaft resistance, which varies inversely with pile diameter. While further refinement is possible, the calculations provide broadly representative predictions that both aid test interpretation and offer a simplified procedure that can assist practical cyclic foundation design.

CONCLUSIONS

Monotonic tests on open steel pipe piles driven in low-to-medium-density chalk for the ALPACA research programme developed monotonic shaft resistances that varied with pile diameter, L/D ratio, age after driving, relative water table depth and loading sense (compression against tension). Comprehensive axial cyclic testing programmes conducted on 14 aged and otherwise undisturbed SD and LD piles led to ten primary conclusions.

(*a*) The field test outcomes yield systematic patterns in normalised cyclic interaction diagrams that allow

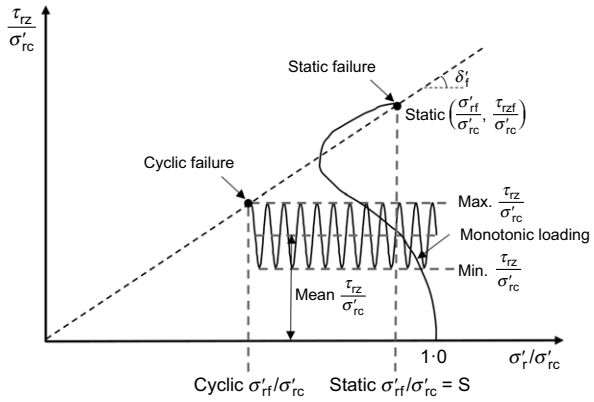


Fig. 15. Schematic diagram of pile shaft failure under monotonic and cyclic loading

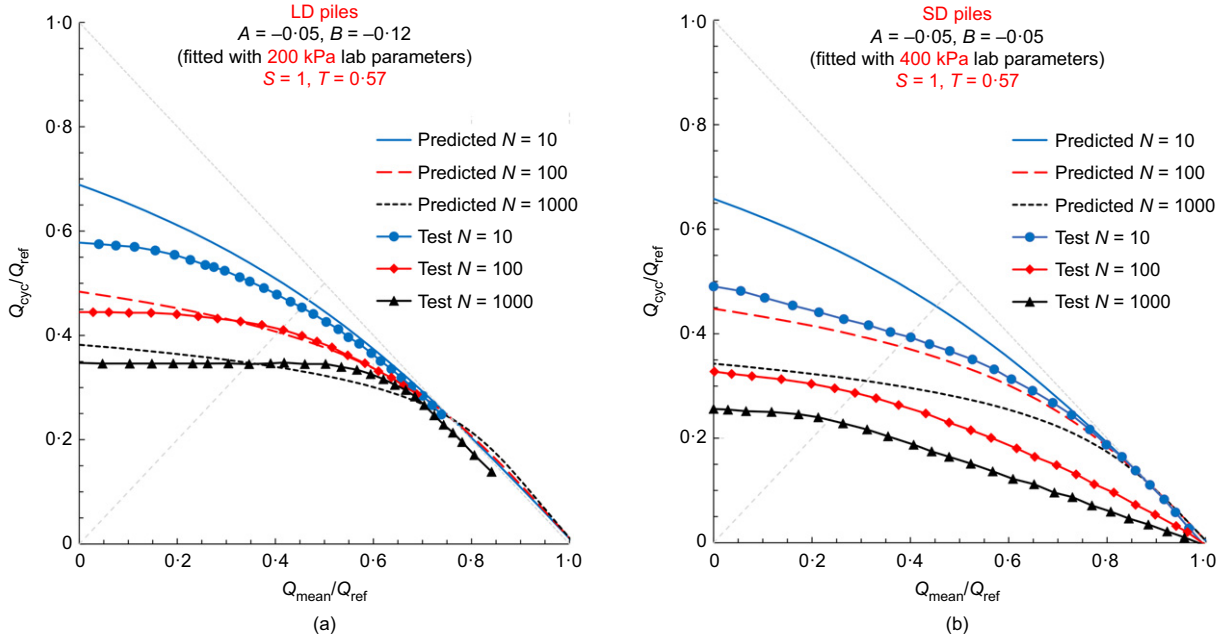


Fig. 14. Predictions for failure contours of: (a) LD piles; (b) SD piles, as set out in Appendix compared with field test outcomes from Fig. 3

Downloaded by [] on [30/05/24]. Published with permission by the ICE under the CC-BY license

contoured representation of the conditions under which either cyclic failure develops under specified numbers of cycles, or stable and metastable conditions apply.

(*b*) The cyclic shaft resistances of the test piles were controlled by the behaviour of, and conditions within, the reconsolidated, de-structured, chalk putty annuli that form around the pile shafts during driving and are constrained radially by the stiff intact chalk mass.

(*c*) Cyclic axial loading degraded shaft resistance most severely under high-level, two-way loading involving low mean loads. This feature may be critical to cyclic foundation design.

(*d*) SD piles were more susceptible, in normalised terms, to severe cyclic loading than LD piles. A FoS $\approx 2{\cdot}9$ was required for LD piles to survive 1000 cycles under extreme two-way conditions, while a factor $\approx 3{\cdot}6$ appeared necessary for SD piles.

(*e*) FBG strain gauge strings identified the patterns of degradation applying in unstable tests as involving progressive failure from the pile tip upwards.

(*f*) Post-cycling monotonic tests to failure confirmed that stable cycling enhances pile capacity marginally, while unstable cases may experience large losses of shaft capacity. Metastable intermediate outcomes involved only minor shaft capacity losses.

(*g*) The patterns by which pile head deflections grew under cyclic loading varied systematically with the normalised axial loading parameters and could be captured by simple fitting expressions.

(*h*) The non-linear pile cyclic stiffnesses varied with loading conditions in a consistent fashion. Checks with elastic theory demonstrated that the highest operational shear stiffnesses that could be interpreted for the chalk mass amounted to approximately 25% of those measured by in situ seismic CPT tests. This trend was ascribed to the Chalk's fissured macrostructure and damage caused by pile driving.

(*i*) Cyclic triaxial tests conducted on chalk putty samples consolidated to conditions comparable to the average states applying around the test piles gave fair 'global' predictions for the pile test failure conditions when combined with laboratory interface shear test outcomes.

(*j*) A trend was noted for the global predictions to be marginally non-conservative, which may be related to unmodelled phenomena such as the piles' top upwards progressive failures. However, the simplified treatment followed appeared to capture the main processes that lead to shaft capacity degradation under cyclic loading.

ACKNOWLEDGEMENTS

The ALPACA project was funded by the Engineering and Physical Science Research Council (EPSRC) through grant EP/P033091/1. The authors acknowledge the provision of additional financial and technical support by the following project partners: Atkins, Cathies, Equinor, Fugro, GCG, Innogy (RWE), LEMS, Ørsted, Parkwind, Siemens-Gamesa, SPR and Vattenfall. The authors acknowledge gratefully the work of Socotec UK Ltd as the main contractor for the LD field-testing programme, Marmota Engineering AG as the subcontracted fibre-optic strain gauge specialist, Green Piling Ltd who installed the piles, and Lankelma UK and Fugro Geo-services who carried out the cone penetration tests and boreholes, respectively. Imperial College's EPSRC Centre for Doctoral Training (CDT) in Sustainable Civil Engineering (EP/L016826/1) and the DEME Group (Belgium) supported Ken Vinck's doctoral study, while Byrne is supported by the Royal Academy of Engineering under the Research Chairs and Senior Research Fellowships scheme.

APPENDIX

A schematic illustration of the local stress paths expected on the pile shaft under monotonic and cyclic loading to failure is given in Fig. 14. Buckley *et al*. (2018b) show that the static shaft shear stress τ_{max} at which driven piles reach failure in chalk satisfy the Coulomb failure criterion.

$$\left(\tau_{rzf}^{max}\right)_{static} = \sigma'_{rf} \tan(\delta'_f) \tag{4}$$

The radial effective stress acting on pile shafts under monotonic failure, σ'_{rf}, in equation (4) is determined by installation and ageing, prior to static loading, which defines σ'_{rc} plus any reduction induced during static loading ($\Delta\sigma'_{rd}$) by principal stress axis rotation and the increases that occur due to constrained dilation, which vary inversely with pile diameter.

$$(\sigma'_{rf})_{static} = \sigma'_{rc} + \Delta\sigma'_{rd} \tag{5}$$

$$S = \frac{(\sigma'_{rf})_{static}}{\sigma'_{rc}} = \frac{(\tau_{rzf}^{max})_{static}}{\sigma'_{rc} \times \tan(\delta'_f)} \tag{6}$$

Under cyclic loading conditions, local shaft cyclic failure initiates when the peak of the cyclic effective stress paths engage the interface failure δ'_f envelope (Tsuha *et al*., 2012), neglecting the impact of pre-shear on σ'_r under cyclic loading.

$$\tan(\delta'_f) = \frac{\left(\tau_{rz}^{max}\right)_{cyclic} / \sigma'_{rc}}{(\sigma'_r)_{cyclic} / \sigma'_{rc}} \tag{7}$$

$$\left(\frac{\sigma'_{rf}}{\sigma'_{rc}}\right) = \frac{\tau_{rz}^{max} / \sigma'_{rc}}{\tan(\delta'_f)} \tag{8}$$

$$\left(\frac{\Delta\sigma'_{rc}}{\sigma'_{rc}}\right) = 1 - \frac{\tau_{rz}^{max} / \sigma'_{rc}}{\tan(\delta'_f)} \tag{9}$$

Cyclic failure is initiated when the stress path engages the interface shear failure criterion, while the static failure can involve a dilatant stage in sands (Tsuha *et al*., 2012). Considering constant-amplitude uniform cycling conditions, the cyclic shear stress at peak τ_{max} ($= \tau_{mean} + \tau_{cyc}$) can be linked with changes in radial effective stress at cyclic failure, $(\Delta\sigma'_{rc})_{cyclic}$, through the following equation.

$$\left(\frac{\Delta\sigma'_{rc}}{\sigma'_{rc}}\right)_{cyclic} = \frac{\sigma'_{rc} - \sigma'_{rf}}{\sigma'_{rc}} = 1 - \frac{\tau_{mean} + \tau_{cyc}}{\sigma'_{rc} \times \tan(\delta'_f)} \tag{10}$$

Combining equations (6) and (10) leads to

$$\left(\frac{\Delta\sigma'_{rc}}{\sigma'_{rc}}\right)_{cyclic} = 1 - S \times \left[\frac{\tau_{mean}}{(\tau_{rzf}^{max})_{static}} + \frac{\tau_{cyc}}{(\tau_{rzf}^{max})_{static}}\right] \tag{11}$$

which can be rearranged as

$$\frac{\tau_{mean}}{(\tau_{rzf}^{max})_{static}} = \frac{1}{S}\left[1 - \left(\frac{\Delta\sigma'_{rc}}{\sigma'_{rc}}\right)_{cyclic}\right] - \frac{\tau_{cyc}}{(\tau_{rzf}^{max})_{static}} \tag{12}$$

Under laboratory cyclic simple shear conditions, the horizontal plane on which cyclic shear stresses are applied is analogous to the vertical soil–pile interface surface and the laboratory axial (vertical) effective stresses acting on the horizontal plane represent the radial effective stresses on the vertical pile shaft; Aghakouchak (2015).

$$\left(\frac{\Delta\sigma'_z}{\sigma'_{z0}}\right)_{Lab\ SS} = \left(\frac{\Delta\sigma'_{rc}}{\sigma'_{rc}}\right)_{Pile} \tag{13}$$

Degradation in radial effective stress component ($\Delta\sigma'_{rc}/\sigma'_{rc}$) under cyclic loading can be gauged directly from the evolving trend of vertical effective stress component (σ'_z) in cyclic simple shear tests (CSS). When cyclic triaxial tests are employed to match 'simple shear' pile interface conditions, the pile shaft shear stress can be

Downloaded by [] on [30/05/24]. Published with permission by the ICE under the CC-BY license

related to the triaxial deviatoric stress changes (Δq) and the variations in triaxial mean effective stress ($\Delta p'$) taken as indicators as to how σ'_{rc} may change close to the pile under cyclic loading. A correction factor T is introduced to correlate changes in mean effective stress under triaxial conditions and vertical effective stress under the simple shear condition.

$$\frac{\Delta p'}{p'_0} = \frac{\Delta \sigma'_z}{\sigma'_{z0}} \times T \tag{14}$$

Figure 16 compares pairs of normalised effective stress paths from (*a*) monotonic triaxial tests by Liu *et al.* (2022) and (*b*) direct simple shear (DSS) tests on normally consolidated, fully de-structured chalk prepared with dynamic compaction to similar void ratios ($\approx 0{\cdot}69$). T falls between 0·50 and 0·64 at the monotonic phase transformation points and the average $T = 0{\cdot}57$ was adopted for this study. A higher T range ($0{\cdot}92 \pm 0{\cdot}08$) was identified by Aghakouchak (2015) from cyclic hollow cylinder simple shear (HCA SS) and triaxial tests on fine, dense, anisotropically overconsolidated Dunkirk and Fontainebleau NE34 sands.

Combining equations (12) and (14) leads to

$$\frac{q_{mean}/2}{(\tau^{max}_{rzf})_{static}} = \frac{1}{S}\left(1 + \frac{\Delta p'}{p'_0} \times \frac{1}{T}\right) - \frac{q_{cyc}/2}{(\tau^{max}_{rzf})_{static}} \tag{15}$$

in which $\Delta p' = p' - p'_0$. Liu *et al.* (2022) report correlations between the changes in p' and the cyclic loading stress components (q_{mean} and q_{cyc}) as

$$\frac{\Delta p'}{p'_0} = A \times \left(B + \frac{q_{cyc}}{p'_0}\right) \times N^C \tag{16}$$

$$C = 3 \cdot 48 \times \frac{q_{cyc}}{p'_0} \tag{17}$$

Tests conducted after consolidation to $p'_0 = 200$ kPa indicated $A = -0{\cdot}05$, $B = -0{\cdot}12$, regardless of the applied q_{cyc}/p'_0 ratio, although they indicated a far wider $0{\cdot}3 < C < 1{\cdot}3$ range than reported for dense sands or stiff clays by Aghakouchak (2015) and Rattley *et al.* (2017). Parallel tests on samples consolidated to $p'_0 = 400$ kPa indicated $B = -0{\cdot}05$, while A and C correlations remain unchanged.

Equation (12) can offer preliminary 'global' predictions from single element tests of the failure conditions of the field cyclic pile tests through:

$$\frac{Q_{mean}}{Q_{ref}} = \frac{1}{S}\left(1 + \frac{\Delta p'}{p'_0} \times \frac{1}{T}\right) - \frac{Q_{cyc}}{Q_{ref}} \tag{18}$$

Applying $Q_{cyc}/Q_{ref} = \tau_{cyc}/(\tau^{max}_{rzf})_{static}$ and $Q_{mean}/Q_{ref} = \tau_{mean}/(\tau^{max}_{rzf})_{static}$, where Q_{ref} denotes the reference monotonic pile shaft capacity.

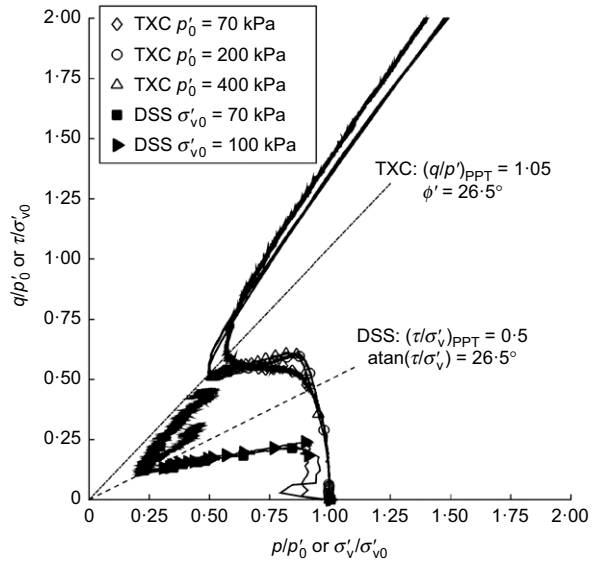


Fig. 16. Normalised effective stress paths of fully de-structured chalk from undrained triaxial and direct simple shear tests

The above simple model gives potentially anomalous results in cases involving a high near-failure Q_{mean} in combination with low Q_{cyc} when $S \neq 1$, although few tests were conducted in this region, which would normally be avoided in design. The constrained dilation component led to $S > 1$ in 102 mm D ICP tests in SNW chalk by Buckley *et al.* (2018b), due mainly to the pile's small diameter and the chalk's high in situ stiffness. In such cases the simplified model can imply improbably significant differences between monotonic and cyclic shaft capacities at failure. For simplicity, S was therefore taken as unity in the present study.

NOTATION

A, B, C	fitting parameters for effective stress degradation
a	accumulated cyclic displacement
D	diameter of pile or penetrometer
f_s	cone penetration test sleeve friction
G_{max}	maximum shear modulus
G_{vh}	shear modulus in the vertical plane
H	distance from the pile tip
k_L	cyclic loading stiffness
k_s	displacement creep rate
k_U	cyclic unloading stiffness
L_p	pile embedded length
N	number of cycles
p'	mean effective stress in triaxial testing
Q_b	pile base capacity
Q_{cyc}	axial cyclic load amplitude
Q_{max}	maximum cyclic load, $= Q_{mean} + Q_{cyc}$
Q_{mean}	mean axial cyclic load
Q_{min}	minimum cyclic load
Q_{pc}	post cyclic tension capacity
Q_{ref}	reference pile static tension capacity
q_{cyc}	cyclic deviatoric stress applied in triaxial testing
q_{max}	maximum deviatoric stress, $= q_{mean} + q_{cyc}$
q_{mean}	mean deviatoric stress in triaxial testing
q_t	cone penetration test cone resistance
R^*	open ended pile effective radius
S, T	parameters in the laboratory-based modelling approach
$S_u^{pre\text{-}PT}$	undrained shear strength defined at phrase transformation
α, β	power law parameters
$\Delta\sigma'_{rd}$	change in radial effective stress in static loading
δ'_f	residual interface friction angle
Λ	set-up factor
σ'_r	radial effective stress
σ'_z	vertical effective stress
τ_{avg}	average shaft resistance
τ_{cyc}	cyclic shear stress
τ_{max}	maximum shear stress
τ_{mean}	mean shear stress
τ_{rz}	total shaft resistance
$(\tau^{max}_{rzf})_{static}$	maximum shaft shear stress at static failure
ϕ'	effective angle of shearing resistance

REFERENCES

Aghakouchak, A. (2015). *Advanced laboratory studies to explore the axial cyclic behaviour of driven piles.* PhD thesis, Department of Civil and Environmental Engineering, Imperial College, London, UK.

Ahmadi-Naghadeh, R., Liu, T., Vinck, K., Jardine, R. J., Kontoe, S., Byrne, B. & McAdam, R. A. (2022). A laboratory characterisation of the response of intact chalk to cyclic loading. *Géotechnique*, https://doi.org/10.1680/jgeot.21.00198.

Atkins (Atkins Consultants Ltd) (2000). *Cyclic degradation of offshore piles*, HSE offshore technology Report OTO 2000 013. Norwich, UK: Her Majesty's Stationery Office.

Barbosa, P. M., Geduhn, M., Jardine, R. J. & Schroeder, F. C. (2017). Large scale offshore static pile tests-practicality and benefits. In *Proceedings of the 8th international conference on offshore site investigation and geotechnics* (ed. T. Powell), pp. 644–651. London, UK: Society for Underwater Technology.

Downloaded by [] on [30/05/24]. Published with permission by the ICE under the CC-BY license

Buckley, R. M. (2018). *The axial behaviour of displacement piles in chalk*. PhD thesis, Department of Civil and Environmental Engineering, Imperial College, London, UK.

Buckley, R. M., Jardine, R. J., Kontoe, S., Parker, D. & Schroeder, F. C. (2018a). Ageing and cyclic behaviour of axially loaded piles driven in chalk. *Géotechnique* **68**, No. 2, 146–161, https://doi.org/10.1680/jgeot.17.P.012.

Buckley, R. M., Jardine, R. J., Kontoe, S. & Lehane, B. M. (2018b). Effective stress regime around a jacked steel pile during installation ageing and load testing in chalk. *Can. Geotech. J.* **55**, No. 11, 1577–1591.

Buckley, R. M., Jardine, R. J., Kontoe, S., Barbosa, P. & Schroeder, F. C. (2020a). Full-scale observations of dynamic and static axial responses of offshore piles driven in chalk and tills. *Géotechnique* **70**, No. 8, 657–681, https://doi.org/10.1680/jgeot.19.TI.001.

Buckley, R. M., McAdam, R. A., Byrne, B. W., Doherty, J. P., Jardine, R. J., Kontoe, S. & Randolph, M. F. (2020b). Optimisation of impact pile driving using optical fibre Bragg grating measurements. *J. Geotech. Geoenviron. Engng* **146**, No. 9, 04020082, https://doi.org/10.1061/(ASCE)GT.1943-5606.0002293.

Burland, J. B. & French, D. J. (1990). Results of trials in weathered chalk of a novel piling system – the wedge pile. In *Chalk: proceedings of the international chalk symposium held at Brighton Polytechnic on 4-7 September 1989*, pp. 375–383. London, UK: Thomas Telford.

Ciavaglia, F., Carey, J. & Diambra, A. (2017a). Monotonic and cyclic lateral tests on driven piles in chalk. *Proc. Instn Civ. Engrs Geotech. Engng* **170**, No. 4, 353–366, https://doi.org/10.1680/jgeen.16.00113.

Ciavaglia, F., Carey, J. & Diambra, A. (2017b). Time-dependent uplift capacity of driven piles in low to medium density chalk. *Géotechnique Lett.* **7**, No. 1, 90–96, https://doi.org/10.1680/jgele.16.00162.

Erbrich, C. T., O'neill, M. P., Clancy, P. & Randolph, M. F. (2010). Axial and lateral pile design in carbonate soils. In *Frontiers in offshore geotechnics II* (eds S. Gourvenec and D. White), pp. 125–154. London, UK: Taylor & Francis Group.

Jardine, R. J. (2020). Geotechnics, energy and climate change: the 56th Rankine Lecture. *Géotechnique* **70**, No. 1, 3–59, https://doi.org/10.1680/jgeot.18.RL.001.

Jardine, R. J. & Standing, J. R. (2012). Field axial cyclic loading experiments on piles driven in sand. *Soils Found.* **52**, No. 4, 723–736.

Jardine, R. J., Puech, A. & Andersen, K. H. (2012). Cyclic loading of offshore piles: potential effects and practical design. In *Proceedings of the 7th international conference on offshore site investigation and geotechnics*, pp. 59–97. London, UK: Society for Underwater Technology.

Jardine, R. J., Buckley, R. M., Kontoe, S., Barbosa, P. & Schroeder, F. C. (2018). Behaviour of piles driven in chalk. In *Engineering in chalk: proceedings of the chalk 2018 conference* (eds J. A. Lawrence, M. Preene, U. L. Lawrence and R. Buckley), pp. 33–52. London, UK: ICE Publishing.

Jardine, R. J., Kontoe, S., Liu, T., Vinck, K., Byrne, B. W., McAdam, R. A., Schranz, F., Andolfsson, T. & Buckley, R. M. (2019). The ALPACA research project to improve design of piles driven in chalk. In *Proceedings of the 17th European conference on soil mechanics and geotechnical engineering* (eds H. Sigursteinsson, S. Erlingsson and B. Bessason), https://doi.org/10.32075/17ECSMGE-2019-0071. Reykjavík, Iceland: The Icelandic Geotechnical Society.

Jardine, R. J., Buckley, R. M., Liu, T., Andolfsson, T., Byrne, B. W., Kontoe, S. J., McAdam, R. A., Schranz, F. & Vinck, K. (2023). The behaviour of piles driven in chalk under axial loading. *Géotechnique*, https://doi.org/10.1680/jgeot.22.00041.

Karlsrud, K., Nadim, F. & Haugen, T. (1986). Piles in clay under cyclic axial loading – field tests and computational modelling. *Proceedings of the 3rd international conference on numerical methods in offshore piling*, Nantes, France, pp. 165–190.

Lahrs, T. & Kallias, A. (2013). Probebelastungen von Stahlrohren in Kreide für den offshore-windpark baltic 2. *Proceedings of the Pfahl symposium*, Braunschweig, Germany, pp. 451–466 (in German).

Liu, T., Ahmadi-Naghadeh, R., Vinck, K., Jardine, R. J., Kontoe, S., Buckley, R. M. & Byrne, B. (2022). An experimental investigation into the behaviour of de-structured chalk under cyclic loading. *Géotechnique*, https://doi.org/10.1680/jgeot.21.00199.

Liu, T., Ferreira, P. M. V., Vinck, K., Coop, M. R., Jardine, R. J. & Kontoe, S. (2023). The behaviour of a low-to-medium density chalk under a wide range of pressure conditions. *Soils Found.* **63**, No. 1, 101268.

Lombardi, D., Bhattacharya, S. & Nikitas, G. (2017). Physical modeling of offshore wind turbine model for prediction of prototype response. In *Wind energy engineering: a handbook for onshore and offshore wind turbines* (ed. T. M. Letcher), pp. 353–374, https://doi.org/10.1016/B978-0-12-809451-8.00017-5. London, UK: Academic Press.

Lord, J. A., Clayton, C. R. L. & Mortimore, R. N. (2002). *Engineering in chalk*. London, UK: CIRIA.

Poulos, H. G. (1988). Cyclic stability diagram for axially loaded piles. *J. Geotech. Geoenviron. Engng* **114**, No. 8, 877–895.

Randolph, M. F. & Wroth, C. P. (1978). Analysis of deformation of vertically loaded piles. *ASCE J. Geotech. Geoenviron. Engng* **104**, No. 12, 1465–1488.

Rattley, M., Costa, L., Jardine, R. J. & Cleverly, W. (2017). Laboratory test predictions of the cyclic axial resistance of a pile driven in North Sea soils. In *Proceedings of the 8th international conference on offshore site investigation and geotechnics* (ed. T. Powell), pp. 636–643. London, UK: Society for Underwater Technology.

Tsuha, C. H. C., Foray, P. Y., Jardine, R. J., Yang, Z. X., Silva, M. & Rimoy, S. (2012). Behaviour of displacement piles in sand under cyclic axial loading. *Soils Found.* **52**, No. 3, 393–410.

Vinck, K. (2021). *Advanced geotechnical characterisation to support driven pile design at chalk sites*. PhD thesis, Department of Civil and Environmental Engineering, Imperial College, London, UK.

Vinck, K., Liu, T., Jardine, R. J., Kontoe, S., Ahmadi-Naghadeh, R., Buckley, R. M., Byrne, B. W., Lawrence, J. A., McAdam, R. A. & Schranz, F. (2022). Advanced in situ and laboratory characterisation of the ALPACA chalk research site. *Géotechnique*, https://doi.org/10.1680/jgeot.21.00197.

Downloaded by [] on [30/05/24]. Published with permission by the ICE under the CC-BY license